Geophys. J. Int. (1994) **118,** 515–528

Shear-wave velocity and attenuation structure beneath Antarctica determined from surface waves

D. D. Singh

National Geophysical Research Institute, Uppal Road, Hyderabad 500 007, *India*

Accepted 1994 January 24. Received 1994 January 24; in original form 1992 July 21

SUMMARY

Fundamental and higher mode surface waves generated by nine earthquakes, which occurred in Antarctica and its nearby regions and were recorded at Scott Base (SBA), South Pole (SPA), Novolazarevskaya (NVL) and Mirnyy (MIR) seismic stations are used to determine the shear-wave velocity and attenuation structure beneath these regions. The Frequency-Time Analysis method is used to determine group velocities for periods ranging from 6 to 80 seconds for fundamental and higher mode Rayleigh and Love waves. Crustal thickness is found to be 41 km beneath the eastern part and 30 km beneath the western part of Antarctica. Rayleigh and Love wave group velocities show lower values in the eastern part as compared to the western part of Antarctica. A shear-wave velocity of 3.52 to 3.7 km s^{-1} is estimated in the lower part of the crust (15–41 km from the surface) beneath eastern Antarctica. Similarly a shear-wave velocity of 3.48–3.6 km s^{-1} is estimated in the lower part of the crust (15–30 km from the surface) beneath western Antarctica. Rayleigh and Love wave group velocities are found to be lower for eastern Antarctica compared to Australia, Canada, India and other shield models of the world.

Love and Rayleigh wave attenuation coefficients are estimated at periods of 10–110 s using the spectral amplitude of these waves across the eastern and western parts of Antarctica. Backus & Gilbert inversion theory is applied to the surface-wave attenuation data to obtain average Q_β^{-1} models for the crust and upper mantle beneath Antarctica. Inversion of Love and Rayleigh wave attenuation data shows a high-attenuation zone ($Q = 125$–200) at a depth of 10 to 40 km beneath eastern Antarctica. Similarly, a high-attenuation zone ($Q = 65$) occurs at a depth of 20 to 90 km beneath western Antarctica. The Q_β^{-1} models show a lithospheric thickness of 80–100 km beneath western Antarctica. The base of the lithosphere is identified as the depth at which there is a significant change in the Q_β^{-1} value. The Q_β^{-1} models for Antarctica show that there is a decrease in Q_β^{-1} value by an average of three factors in the asthenosphere as compared to lithosphere. In general, Q_β^{-1} in the asthenosphere show a higher value (an average of 2–3 times) compared to the lithosphere. This implies that the asthenosphere beneath Antarctica is cooler compared to other shield structures of the world.

Key words: Antarctica, dispersion, Q structure.

INTRODUCTION

The dispersive properties of seismic surface waves have been used in the past to determine the crust and upper mantle velocity structure beneath Antarctica, by several workers (Evison *et al.* 1960; Kovach & Press 1961; Dewart & Toksoz 1965; Knopoff & Vane 1978/79). However, the dispersive technique has been hindered by the lack of earthquakes located to provide purely continental paths in Antarctica between epicentres and the few Antarctic stations equipped with long-period seismographs. In determining the group velocities accurately across Antarctic continents, paths with considerable oceanic portions had to be used and errors due to uncertainties in proper corrections for the oceanic fractions of the total path have to be accounted for for this purpose. However, there are pure oceanic paths in the present study and these have been used in calculating the group velocity across the oceanic region. It

has helped us in correcting the observed dispersion data for the pure Antarctic paths. It is very difficult to consider only pure continental paths, as there are not many earthquakes located in the Antarctic. In view of these difficulties, we have selected nine earthquakes that occurred in Antarctica and its vicinity, and that were recorded at South Base (SBA), South Pole (SPA), Novolazarevskaya (NVL) and Mirnyy (MIR) seismic stations and used the surface-wave portions of the seismogram to determine the shear-wave velocity and attenuation (Q_β^{-1} models) structure for eastern and western Antarctic paths. The division of eastern and western part refers to the hemispheres in which the two major lobes of the Antarctic land mass more or less lie. East Antarctica represents mainly elevated ancient-shield-type structure and west Antarctica is a complex tectonic unit consisting of small crustal blocks represented geographically as shallow seas. Both the eastern and western parts of Antarctica are covered by an ice cap of 2 to 4 km thickness. As seismic-wave attenuation is more sensitive to variation in temperature and partial melting than velocity, mapping of Q structure along with shear-wave velocity information beneath Antarctica will be useful to understand the mechanism of breakup of Gondwanaland in the past.

DATA ANALYSIS

The details of the earthquakes are listed in Table 1. The earthquake parameters have been taken from either International Seismological Centre (ISC) bulletins or National Oceanic and Atmospheric Administration (NOAA) tape file. The various wave-propagation paths are shown in Fig. 1 and are listed in Table 1. The surface waves are digitized at irregular time intervals and interpolated at time intervals of 0.25 s using Lagrangian interpolation. The long-period vertical-component records are used for the Rayleigh wave. The long-period north–south and east–west components are rotated to obtain transverse components, which are used for Love waves. The linear trend and arithmetic mean are removed from the digitized data, and the data are tapered at both ends. The data are corrected for the amplitude and instrumental phase shift (Hagiwara 1958). The Frequency-Time Analysis (FTAN) technique by Nyman & Landisman (1977) is used to estimate the group velocity of fundamental and higher mode Rayleigh and Love waves for various propagation paths of the eastern and western Antarctic. The correction for the oceanic path (non-Antarctic part) is done using the relation given by Singh (1988). The following relation is used for correcting the group velocity of the non-Antarctic path:

$$\frac{1}{U}=\frac{r}{U_1}+\frac{(1-r)}{U_2}. \tag{1}$$

Here, U = group velocity of the mixed (Antarctic and non-Antarctic) path.
U_1 = group velocity of Antarctic path.
U_2 = group velocity of non-Antarctic path.
r = portion of path of Antarctic region.
$(1-r)$ = portion of path of non-Antarctic region.

Figures 2(a) and (b) show the observed fundamental and higher mode Rayleigh and Love wave group velocities at periods of 6 to 80 s.

Table 1. Parameters of earthquakes used in the present study with various paths to different seismic stations for Love- and Rayleigh-wave dispersion and attenuation studies.

Serial No.	Date	Origin Time (UTC)	Epicentre Lat. °S	Epicentre Long °E/W	Depth (km)	Magnitude m_b	Magnitude M	Seismic stations (Division of Western Antarctica (WA)/ Eastern Antarctica (EA) paths)
1	May 09,1971	08:25:01.7	39.78	104.8 W	95	6.2	6.	SBA,SPA,NVL (WA)
2	May 09,1971	18:35:17.	39.72	104.9 W	95	5.4	5.4	SBA,SPA (WA)
3	May 03 ,1973	23:11:05.7	46.14	73.2 E		5.5	5.5	SBA,SPA,NVL,MIR (EA)
4	Oct. 15 ,1974	03:12:55.3	52.74	27.5 E	33	4.4		SBA,SPA (EA)
5	Oct. 15 ,1974	07:31:42.	70.52	161.53 E	33	4.9		SBA,SPA (EA)
6	Jan. 11 ,1976	23:22:40.5	46.48	101.07 W		5.6	5.	SBA (WA) ,MIR (EA)
7	Feb. 05 ,1977	03:29:18.9	66.45	82.58 W		6.2	6.4	SPA (WA)
8	Nov. 07 ,1979	11:31:49.6	62.58	72.91 W		5.1		SBA,SPA (WA)
9	Nov. 07 ,1979	14:03:52.	60.3	14.2 W		4.9		SBA,SPA,NVL (WA) ,MIR (EA)

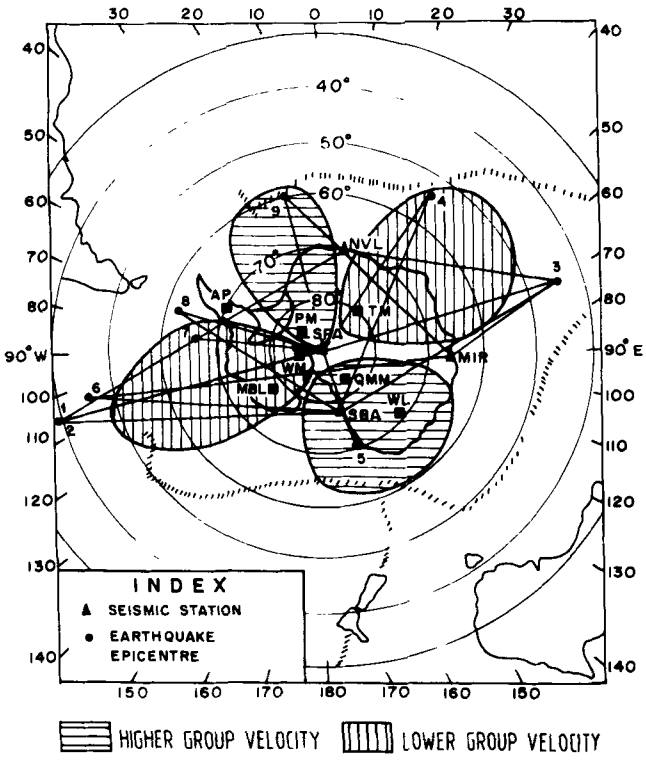

Figure 1. Surface-wave dispersion and attenuation paths used in the study. Earthquake epicentres are indicated by circles, seismic stations by triangles, and Rayleigh wave group velocity by hatched area. (WM = Whitmore Mountains; MBL = Marie Byrd Land; TM = Transantarctic Mountains; QMM = Queen Maud Mountains; WL = Wilkes Land; PM = Pensacola Mountains; AP = Antarctic Peninsula; SBA = Scott Base; SPA = South Pole; NVL = Novolazarevakaya; MIR = Mirnyy.)

The spectral amplitude estimated earlier using the FTAN technique is used for the calculation of attenuation coefficients during the period of 10 to 110 s. The total number of data points is taken to be 4096 ($=2^{12}$). In case the signal is less than this number, the remaining points are taken as zeros to make 4096 points. The attenuation coefficients (Y) of fundamental-mode Rayleigh and Love waves are estimated using different pairs of stations that lie on the same great circle path (with a maximum deviation of 5° on the same alignment for the pair of stations for the same earthquake) using the relation:

$$Y = \frac{\ln\left[\{A_2(\omega, r)/A_1(\omega, r)\}\{\sqrt{(\sin \Delta_2/\sin \Delta_1)}\}\right]}{r_2 - r_1}. \qquad (2)$$

Here r is the epicentral distance in km, Δ is epicentral distance in degrees, ω is angular frequency, A is spectral amplitude, and subscripts 1 and 2 indicate the first and second stations, respectively.

There are various types of errors, which may affect the determination of group velocity and attenuation coefficients of surface waves. They are due to: (1) mislocation of earthquake epicentres, uncertainty in origin time, interference by other phases, improper instrumental correction, lateral refraction, improper separation of modes, and incorrect choice of filter parameter. (2) Other random errors may be caused due to digitization, uncertainties in focal mechanism and presence of a poor signal-to-noise ratio. Singh (1987) has shown that these errors (type one) will correspond to about 0.04 km s^{-1} in group-velocity estimate, or less than 1 per cent. Table 2 lists the fundamental-mode Rayleigh and Love wave group velocities at different time periods along with standard deviations.

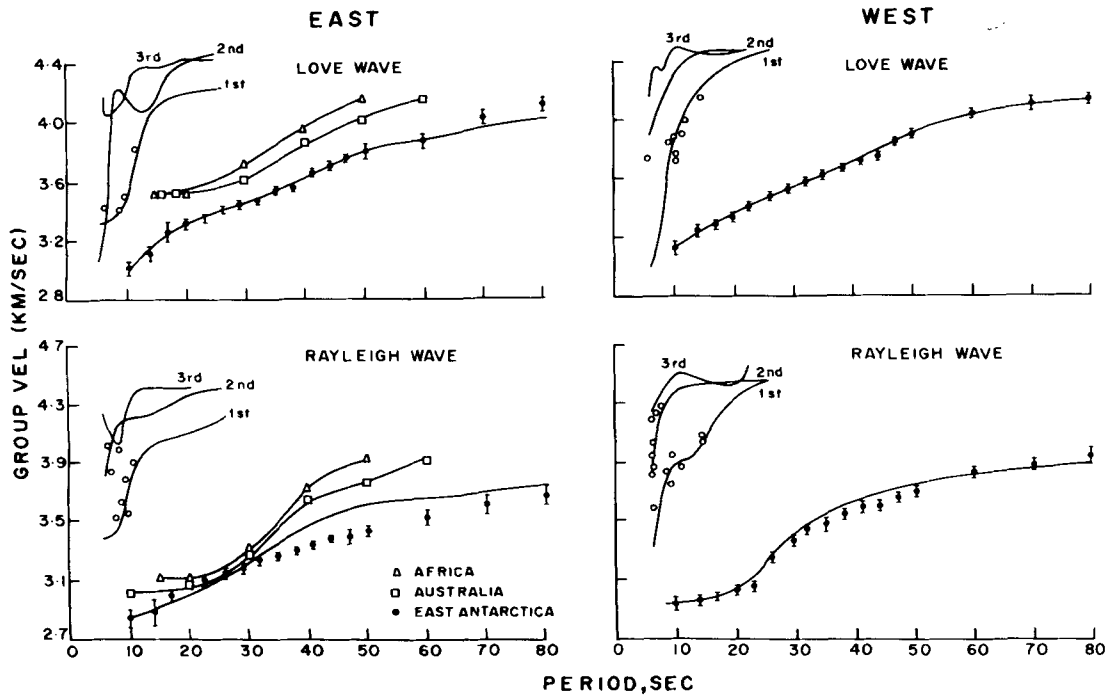

Figure 2(a). Mean and standard deviations of Love and Rayleigh wave group-velocity curves across eastern and western Antarctica. Standard deviations are indicated on each side of the mean values by vertical lines. The theoretical curve is shown as a continuous line. Higher mode dispersion data are shown by open circles. Dispersion curves for Africa (adapted from Bloch, Hales & Landisman 1969) and Australia (adapted from Gonez, Hales & Muirhead 1975) are shown by triangles and squares, respectively.

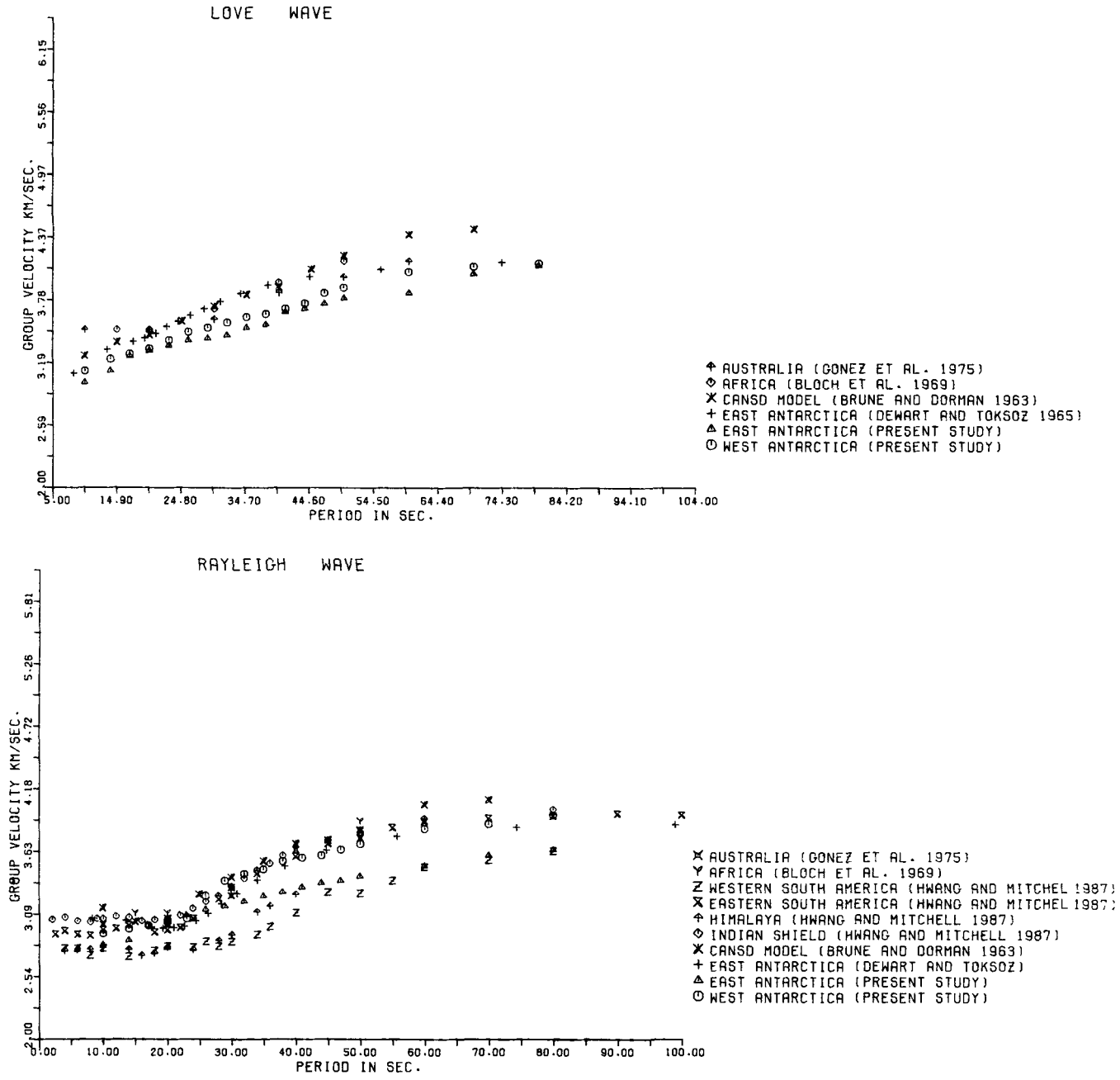

Figure 2(b). Fundamental-mode Rayleigh and Love wave dispersion curves for eastern and western Antarctica are compared with the Australian, African, Indian and Canadian shield (CANSD) models.

INVERSION OF GROUP VELOCITY

A best fit shear-wave velocity model is obtained by the trial and error method of comparison of theoretical and observed data. The dispersion method gives reliable information about the shear-wave velocity structure only. The theoretical dispersion curve is not sensitive to small changes of *P*-wave velocity in different layers. This method is very sensitive to *S*-wave velocity change in different layers. A FORTRAN program was written to generate random models within the specified limits, and group-velocity curves for these models are computed using the exact computation procedure using the Thomson–Haskell matrix formulation (Hwang & Mitchell 1987) (i.e. not using the partial derivatives). Table 3 lists the search limits for different layer parameters (layer thickness, *P*-wave and *S*-wave velocities, and density). The theoretical group velocities for randomly generated models are compared with the observed values. Several thousand models are tested for this ad hoc forward modelling and the selected model is that which gives best fit to both Love and Rayleigh wave group velocities. The criteria for the selection of the best fit model is done both for Love and Rayleigh wave group velocities. The model that gives minimum RMS error between the observed

Table 2. Mean and standard deviations of fundamental-mode Rayleigh and Love wave group velocity ($km\,s^{-1}$) across Antarctica.

Period	Eastern Antarctica				Western Antarctica			
(sec.)	Love		Rayleigh		Love		Rayleigh	
	Mean	S.D.	Mean	S.D.	Mean	S.D.	Mean	S.D.
10	3.0	0.1	2.82	0.12	3.11	0.12	2.92	0.1
14	3.11	0.11	2.86	0.16	3.22	0.1	2.96	0.05
17	3.25	0.12	2.99	0.04	3.27	0.07	2.99	0.07
20	3.3	0.03	3.04	0.07	3.32	0.05	3.02	0.04
23	3.35	0.01	3.08	0.06	3.4	0.02	3.05	0.01
26	3.4	0.06	3.13	0.08	3.48	0.01	3.25	0.08
29	3.42	0.05	3.16	0.07	3.52	0.06	3.38	0.06
32	3.45	0.06	3.2	0.06	3.57	0.05	3.44	0.08
35	3.52	0.03	3.25	0.05	3.62	0.04	3.48	0.1
38	3.55	0.04	3.28	0.04	3.65	0.02	3.55	0.08
41	3.67	0.07	3.32	0.03	3.7	0.01	3.58	0.06
44	3.7	0.05	3.36	0.02	3.75	0.04	3.6	0.06
47	3.75	0.08	3.38	0.11	3.85	0.03	3.65	0.06
50	3.8	0.1	3.42	0.1	3.9	0.04	3.7	0.01
60	3.85	0.12	3.51	0.09	4.05	0.06	3.83	0.06
70	4.03	0.11	3.6	0.11	4.1	0.12	3.87	0.08
80	4.11	0.1	3.65	0.11	4.13	0.08	3.95	0.12

dispersion and that calculated from the assumed theoretical models at all the time periods is considered to be the best fit model. The fit for Rayleigh wave group velocity data is not good for the east Antarctica path at periods greater than 30 s, while Love wave data show better fit (Fig. 2a). This may be due to the presence of material/structural heterogeneity below Moho depth. Fig. 2(a) shows the observed and theoretical Love and Rayleigh wave group velocity curves with their standard deviation estimates and Fig. 2(b) shows the comparison of dispersion curves with other shield models of the world. Standard deviation associated with dispersion values are calculated using the

Table 3. Search limit and fixed parameters for ad hoc forward modelling.

Serial No.	Layer thickness (km)	P-wave velocity (km/sec)	S-wave velocity (km/sec)	Density (gm/cm^3)
1	2 - 4	3.6- 4.1	1.8 - 2.4	0.90 (Ice)
2	2 - 4	5.5- 6.0	3.0 - 3.5	2.67
3	6 -12	6.1 -6.4	3.4 - 3.6	2.74
4	7 -12	6.2- 6.6	3.5 - 3.7	2.81
5	6 -18	6.4 -6.7	3.5- 3.8	3.0
6	30 -50	7.8- 8.1	4.1 - 4.6	3.41
7	60 -80	8.0- 8.3	4.2 - 4.8	3.45
8	90 -120	8.1 -8.3	4.3- 4.9	3.47
9	90 -120	8.2 -8.4	4.4 - 5.1	3.5
10	90- 120	8.4- 8.6	4.5 - 5.1	3.6
11	∞	8.6	4.9	3.65

standard formula given by the following relation:

$$\sigma_{i'}^{1} = \left\{ \frac{1}{N-1} \sum_{i'=1}^{N} (G_{i'} - \bar{G})^2 \right\}^{1/2}. \quad (3)$$

Here $\sigma_{i'}^{1}$ is the standard deviation at each time period; N is the total number of dispersion values observed at each period; G_i is the individual observed dispersion value and $\bar{G}$ is the mean of the population.

The standard deviation in each layer of the model is calculated using the relation given by Mitchell (1976) for the stochastic approach to the inverse problem:

$$\sigma_{pi'}^{*} = \left[\sigma^2 W_i^2 \sum \frac{\lambda_i V_{ij}}{(\lambda^2 + \sigma^2)} \right]^{1/2}. \quad (4)$$

The resolution matrix, **R** is calculated using the relation

$$\mathbf{R} = \mathbf{HA} \quad (5)$$

$$\mathbf{H} = \mathbf{\Lambda V^{-1} U^{T}}. \quad (6)$$

Matrix **A** is the partial derivative of group velocity with respect to shear-wave velocity (Rodi *et al.* 1975) and using singular-value decomposition (Lawson & Hansons 1974) is written as

$$A_{m\times n} = U_{m\times n} \Lambda_{m\times n} V^{T}_{n\times n}.$$

In the above equations, W_i = the weight in each layer and is inversely proportional to layer thickness, λ is a damping factor, U = the eigenvectors associated with the column of **A**, V = the eigenvectors associated with rows of **A**, Λ = the diagonal matrix of non-zero eigenvalues of the matrix **A**, **H** = the pseudo-inverse matrix, and σ is the problem variance. The rows of **R** represent the resolving kernels. The best fit models for eastern and western Antarctica with the standard deviations in each layer are listed in Table 4 and are shown in Figs 2(a), (b) and 3 along with other shield models.

INVERSION OF ATTENUATION DATA

Shear-wave dissipation factor, Q_{β}^{-1} of surface waves over a layered medium at a given period is equal to the sum of the dissipation in each layer, assuming $Q_{\beta}^{-2}(Z)$ is smaller (Anderson & Archambeau 1964). The surface-wave attenuation coefficient values and their standard deviations at different time periods can be used to estimate $Q_{\beta}^{-1}(Z)$ models as a function of depth. Mitchell (1975) modified the relations given by Anderson, Ben-Menahem & Archambeau (1965) for calculating the attenuation of dispersed surface waves. The attenuation coefficients for Love and Rayleigh waves are related to the dissipation factors for P and S waves and the partial derivatives of Love and Rayleigh wave phase velocities with respect to shear and compressional wave velocities. These equations are expressed as follows:

$$\Upsilon_{L} = \frac{\pi}{T} \sum_{i=1}^{N} \left(\frac{\beta_i}{C_L^2} \frac{\partial C_L}{\partial \beta_i} \right)_{fd} Q_{\beta i}^{-1}. \quad (7)$$

$$\Upsilon_{R} = \frac{\pi}{T} \left[\sum_{i=1}^{N} \left(\frac{\alpha_i}{C_R^2} \frac{\partial C_R}{\partial \alpha_i} \right)_{fd\beta} Q_{\alpha i}^{-1} + \sum_{i=1}^{N} \left(\frac{\beta_i}{C_R^2} \frac{\partial C_R}{\partial \beta_i} \right)_{fd\alpha} Q_{\beta i}^{-1} \right]. \quad (8)$$

Table 4. Layer parameters for the best fit model across eastern and western Antarctica.

(a) EASTERN ANTARCTICA

Serial No.	Layer thickness (km)	P-wave Velocity (km/sec)	S-wave Velocity ± S.D. (km/sec)	Density (gm/cm^3)
1	3.	3.8	2.0 ±0.06	0.90 (Ice)
2	4.	5.8	3.1 ±0.02	2.67
3	8.	6.3	3.52 ±0.04	2.74
4	10.	6.4	3.62 ±0.05	2.81
5	16.	6.6	3.7 ±0.03	3.0
6	40.	7.9	4.3 ±0.02	3.41
7	70.	8.0	4.35 ±0.01	3.45
8	100.	8.1	4.55 ±0.04	3.47
9	100.	8.3	4.65 ±0.03	3.5
10	100.	8.4	4.7 ±0.02	3.6
11	∞	8.6	4.9	3.65

(b) WESTERN ANTARCTICA

1	3.	3.8	2.0 ±0.08	0.9 (Ice)
2	2.	5.8	3.35 ±0.03	2.67
3	10.	6.3	3.48 ±0.04	2.74
4	8.	6.4	3.55 ±0.05	2.81
5	7.	6.6	3.6 ±0.02	3.0
6	40.	7.9	4.3 ±0.06	3.41
7	70.	8.0	4.5 ±0.04	3.45
8	100.	8.1	4.6 ±0.03	3.47
9	100.	8.3	4.65 ±0.02	3.5
10	100.	8.4	4.75 ±0.01	3.6
11	∞	8.6	4.9	3.65

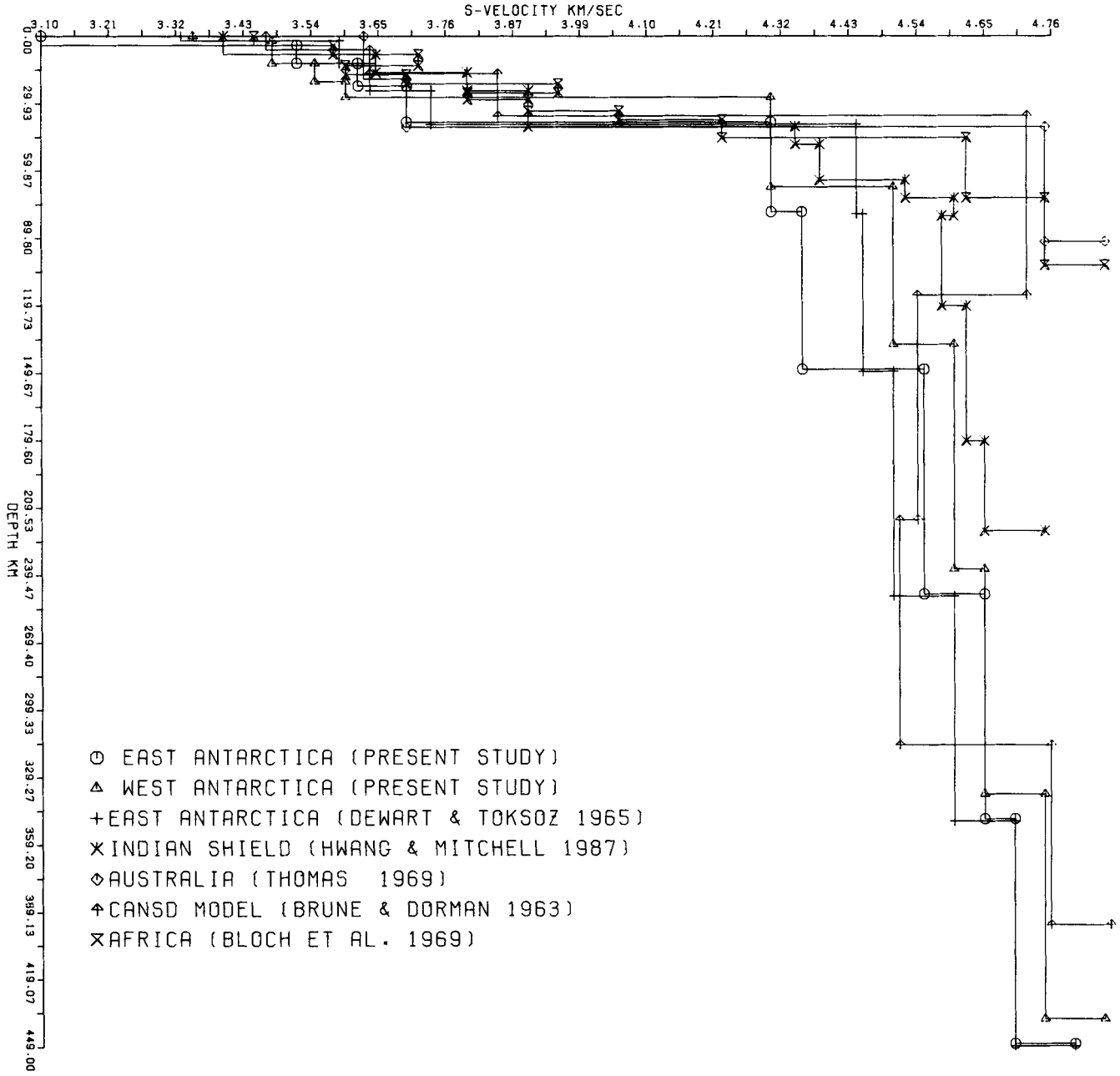

Figure 3. Final selected velocity models for eastern and western Antarctica obtained in the present study are compared with velocity models of the African, Australian and Canadian (CANSD) shield models. Ice thickness in the upper crustal layer is not shown in Antarctica.

Here,

α = *P*-wave velocity.
β = *S*-wave velocity.
C_L = Love wave phase velocity.
C_R = Rayleigh wave phase velocity.
i = Layer index.
N = Number of layers.
Υ_L = Love wave attenuation coefficient.
Υ_R = Rayleigh wave attenuation coefficient.
Q_α = *P*-wave dissipation factor.
Q_β = *S*-wave dissipation factor.

The subscripts f, α, β and d refer to the frequency, *P*-wave velocity, *S*-wave velocity and density, which are held constant. Partial derivatives of Rayleigh and Love wave phase velocities with respect to *P*- and *S*-wave velocities, are computed (Harkrider 1968) for the velocity models determined earlier for eastern and western Antarctica.

Surface-wave attenuation is more sensitive to the shear-wave dissipation factor, Q_β as compared to the *P*-wave dissipation factor, Q_α. For this reason, we have considered Q_β^{-1} values only for the inversion and Q_α is assumed to be twice as large as Q_β at all depths (Anderson

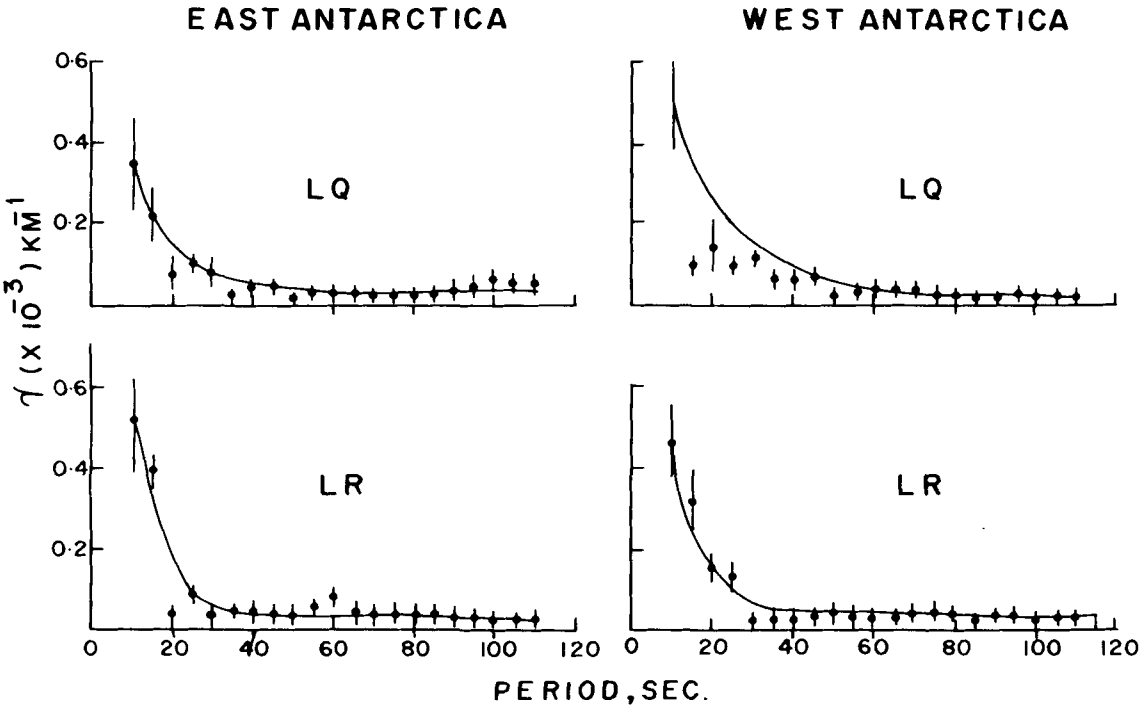

Figure 4. Comparison of observed attenuation coefficients (dots) and 95 per cent confidence limits for eastern and western Antarctica with theoretical values (continuous line) corresponding to the models derived from the separate inversion of Love and Rayleigh wave attenuation data.

et al. 1965). Backus & Gilbert (1970) inversion theory is applied to eqs (7) and (8) in a stochastic form as discussed by Mitchell (1975). This inversion yields a model for $Q_\beta^{-1}(Z)$ at different depths along with the resolving kernels and theoretical attenuation coefficients at different time periods. A large number of trial solutions are made by considering different values of the variance (σ) of the model parameters. In other words, different theoretical attenuation coefficients are calculated by changing the variance (σ) values, and compared with the observed values of attenuation coefficients to match at different time periods. In this process, a number of inversion attempts are made to get the better fit of the theoretical attenuation coefficient values with the observed data. The final model is selected by comparing the theoretical and observed attenuation coefficients for surface waves, which fit the data well. Fig. 4 shows the comparison of observed and theoretical computed attenuation coefficients at time periods of 10 to 110 s for the best fit model, and observed attenuation coefficient values along with standard deviations are listed in Table 5. The variance (σ) is an adjustable parameter that is used to effect a trade-off between the resolution and standard deviations of the model. The layer thickness in the velocity model is divided into a number of layers of 2–5 km thickness with the same layer parameters (P velocities, S velocities and density). Fig. 5 shows the models resulting from these inversions along with the standard deviation of the model at each layer. These models produce a fairly good fit to both Rayleigh and Love wave attenuation data (Fig. 4). Narrow and sharp peaks of resolving kernels at proper depth sections indicate a high degree of resolution, where as broad peaks are indicative of poor resolution. Kernels generated in the inversion process for the selected best fit model indicate that the resolution is good up to 150 km depth, as the peaks are sharper and narrower up to this depth.

$Q_\beta^{-1}(Z)$ have been obtained for eastern and western Antarctica by separate inversion of Rayleigh and Love wave attenuation data. Fig. 5 shows the Q structure for eastern and western Antarctica. A high attenuation zone ($Q = 125$–200) is centred at a depth of 10–40 km beneath eastern Antarctica. Similarly, the high attenuation zone ($Q = 65$) is centred at a depth of 20–90 km beneath western Antarctica.

DISCUSSION

Group-velocity distribution maps have been prepared using the surface-wave tomography (Yanovskaya *et al.* 1988) at periods of 30 and 50 s. For eastern and western Antarctica (Fig. 6). In the surface-wave tomography studies, we have considered all the paths (Fig. 1) of the present study along with the published data of Dewart & Toksoz (1965), Evison *et al.* 1960, and Kovach & Press (1961), in constructing the Rayleigh wave group-velocity distribution map in Antarctica. Fig. 6 shows lower values of group velocity in the region of the Transantarctic Mountains, and higher values of group velocity in the Queen Maud Mountains, Wilkes Lands regions of eastern Antarctica. Similarly, lower values of group velocity are found in the Antarctic Peninsula, Whitmore Mountain, Marie Byrd Land regions, and higher values of group velocity in the Pensacola Mountain region of Western Antarctica (Fig. 1). The lower group-velocity zone extends from a north-east to south-west direction, and the higher group-velocity zone from a north-west to

Table 5. Rayleigh and Love wave attenuation data for the eastern and western Antarctica.

Period (sec.)	RAYLEIGH WAVE				LOVE WAVE			
	East		West		East		West	
	Mean	S.D.	Mean	S.D.	Mean	S.D.	Mean	S.D.
	($X10^{-3}$ km^{-1})				($X10^{-3}$ km^{-1})			
10	0.485	0.24	0.427	0.356	0.358	0.436	0.502	0.231
15	0.556	0.10	0.42	0.22	0.333	0.248	0.158	0.153
20	0.065	0.07	0.292	0.166	0.159	0.112	0.307	0.321
25	0.212	0.23	0.335	0.437	0.251	0.084	0.267	0.01
30	0.098	0.056	0.079	0.029	0.259	0.296	0.384	0.015
35	0.167	0.127	0.132	0.013	0.076	0.05	0.211	0.228
40	0.22	0.219	0.145	0.167	0.185	0.177	0.275	0.138
45	0.167	0.143	0.188	0.057	0.254	0.302	0.369	0.307
50	0.210	0.231	0.291	0.374	0.05	0.014	0.089	0.07
55	0.332	0.391	0.183	0.224	0.107	0.128	0.203	0.058
60	0.558	0.582	0.141	0.087	0.150	0.002	0.349	0.264
65	0.349	0.157	0.32	0.415	0.12	0.113	0.284	0.032
70	0.278	0.235	0.393	0.518	0.072	0.079	0.255	0.064
75	0.276	0.40	0.393	0.518	0.091	0.052	0.196	0.062
80	0.455	0.622	0.357	0.364	0.107	0.028	0.111	0.153
85	0.506	0.322	0.242	0.305	0.318	0.011	0.05	0.028
90	0.318	0.439	0.233	0.088	0.382	0.281	0.178	0.125
95	0.229	0.345	0.194	0.124	0.466	0.321	0.329	0.314
100	0.179	0.189	0.183	0.04	0.662	0.887	0.191	0.156
105	0.197	0.235	0.185	0.084	0.696	0.725	0.103	0.086
110	0.312	0.224	0.237	0.048	0.628	0.764	0.144	0.099

south-east part of Antarctica (Fig. 1). The existence of a lower group velocity at the period of 30 and 50 s is indicative of the presence of a low-velocity zone in the upper mantle below Moho depth. Fig. 5 shows a high attenuation zone centred at shallow depth both for east and west Antarctica. The present selected velocity model (Table 4) does not show the low-velocity zone below Moho depth. It can be explained by the changes in the chemical constitution taking place in the uppermost mantle. The Moho boundary is not sharply defined here, but it represents a gradual transformation of material below Moho depth. The material just above and below the Moho has changed into higher shear-wave velocity due to the presence of higher temperature and pressure conditions prevailing at the shallower depth. The experimental results on olivine at high pressure, and temperature conditions, have shown that the compositional change in this mineral (decrease of the forsterite concentration and increase of that of the fayalite, i.e. increasing of the iron content) causes the increase of the density and decrease of seismic-wave velocity simultaneously, the vice versa. Berg, Moscali & Herg 1989 have documented a petrologically determined crustal geotherm from a continental-rift environment in the Ross Sea and adjacent Transantarctic Mountains. This geotherm is based

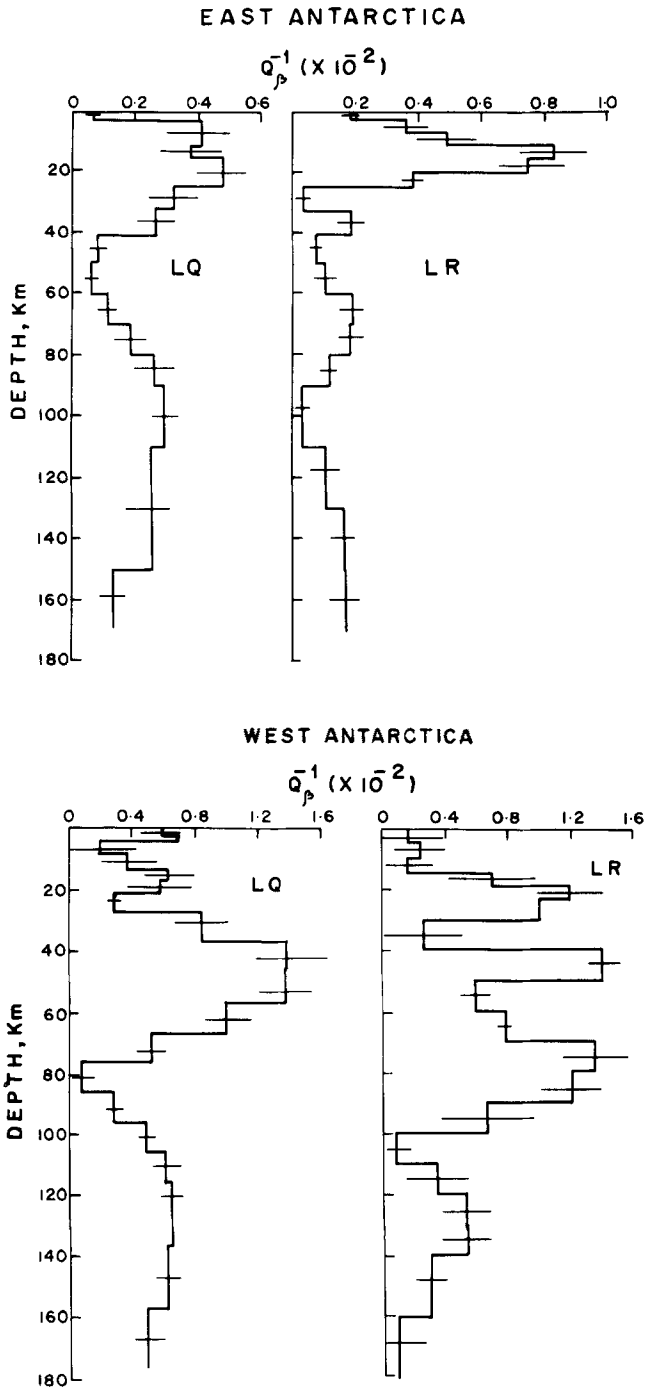

Figure 5. Models resulting from the separate inversion of Love and Rayleigh wave attenuation data and the standard deviation of the model (horizontal bars) for each layer.

on themobarometry of granite, spinel and olivine granulites included in Cenozoic alkaline volcanic rocks. This barometry yields pressures that are in good agreement with Moho depth in the Transantarctic Mountains (40–43 km) and the Ross Embayment (20–28 km). The thermometry yields very high temperatures (900–1000 °C) in the middle and lower crusts. Further, Berg *et al.* 1989 have determined the high geothermal gradient of at least 50–100 °C km^{-1} in this region. The present study also shows higher attenuation at the shallow depth (Fig. 5), which supports the presence of the mantle-plume hypothesis below eastern Gondwana for the breakup of the continent and the evolution of volcanic margins of Antarctica. The sinking of the lithosphere–asthenosphere boundary further down has given large heterogeneity and lateral structural variation below Moho depth. There are several hypothesises for the breakup of Antarctica. Behrendt *et al.* 1991 have suggested that the Gondwana breakup and the west Antarctic rift system were part of a continuously operating single system. There was a progression in rifting and separation around east Antarctica. Behrendt *et al.* 1991 have proposed that this rifting has propagated into west Antarctica (with a spreading-centre jump) to its present location in the Ross Embayment and west Antarctica. Smith & Drewry (1984) have proposed that the rise of the Transantarctic Mountains is a delayed effect caused by overriding east Antarctica of a hot spot that formed under west Antarctica in late Cretaceous time, resulting in phase changes in the upper mantle leading to uplift. Fitzgerald *et al.* 1986 have proposed a simple shear model for uplift of the transantarctic Mountains and extension observed in the basins beneath the Ross Sea shelf and estimated about 200 km (20–30 per cent) of extension, assuming an average of 25–30 km crustal thickness. Stern & ten Brink (1989) have proposed a model in which two lithospheric plates of vastly different effective thermal ages are juxtaposed. Further, they estimate flexure rigidities of 1×10^{25} and 4×10^{22} NM for the two plates, east Antarctica and the extended crust underlying the Ross embayment, respectively. Their corresponding lithospheric elastic thicknesses are 115 ± 10 km and 19 ± 5 km, respectively.

Figure 2(a) shows the comparison of observed dispersion for Antarctica with Australia and Africa, and Fig. 2(b) shows the comparison with other shield areas. The surface-wave group velocities for Antarctica are lower than the stable shield models of the world in the period range of 6 to 80 s. Fig. 3 shows the comparison of the S-wave velocity structure of eastern and western Antarctica with the African and Canadian (CANSD) shield models. The shear-wave velocity is less in the crust and upper mantle for Antarctica than in the stable shield structures of the world. The shear-wave velocities below the Moho vary from 4.43 km s^{-1} to 4.65 km s^{-1} in the Indian shield, 4.75 km s^{-1} in the Australian shield, 4.72 km s^{-1} to 4.76 km s^{-1} in the Canadian shield (CANSD), and 4.62 km s^{-1} to 4.75 km s^{-1} in the African shield regions (Fig. 3). The crustal thickness and shear-wave velocity below Moho depth are the same in the Indian shield and eastern Antarctica. The crustal thickness is estimated to be 41 km beneath the eastern part and 30 km beneath the western part of Antarctica. Rayleigh and Love wave group velocities are lower in the eastern part as compared to the western part of Antarctica. A shear-wave velocity of 3.52 to 3.7 km s^{-1} is estimated in the lower 15–41 km of the crust beneath eastern Antarctica and 3.48–3.6 km s^{-1} in the lower 15–30 km of the crust beneath western Antarctica. The lower shear-wave velocity in the crust and sub-Moho has been reported for eastern Antarctica by other workers also (Evison *et al.* 1960; Kovach & Press 1961; Dewart & Toksoz 1965). Knopoff & Vane (1978/79) have calculated the phase velocity across the eastern Antarctica path and found the crust and upper mantle to be similar to other ancient Precambrian shield areas of the world.

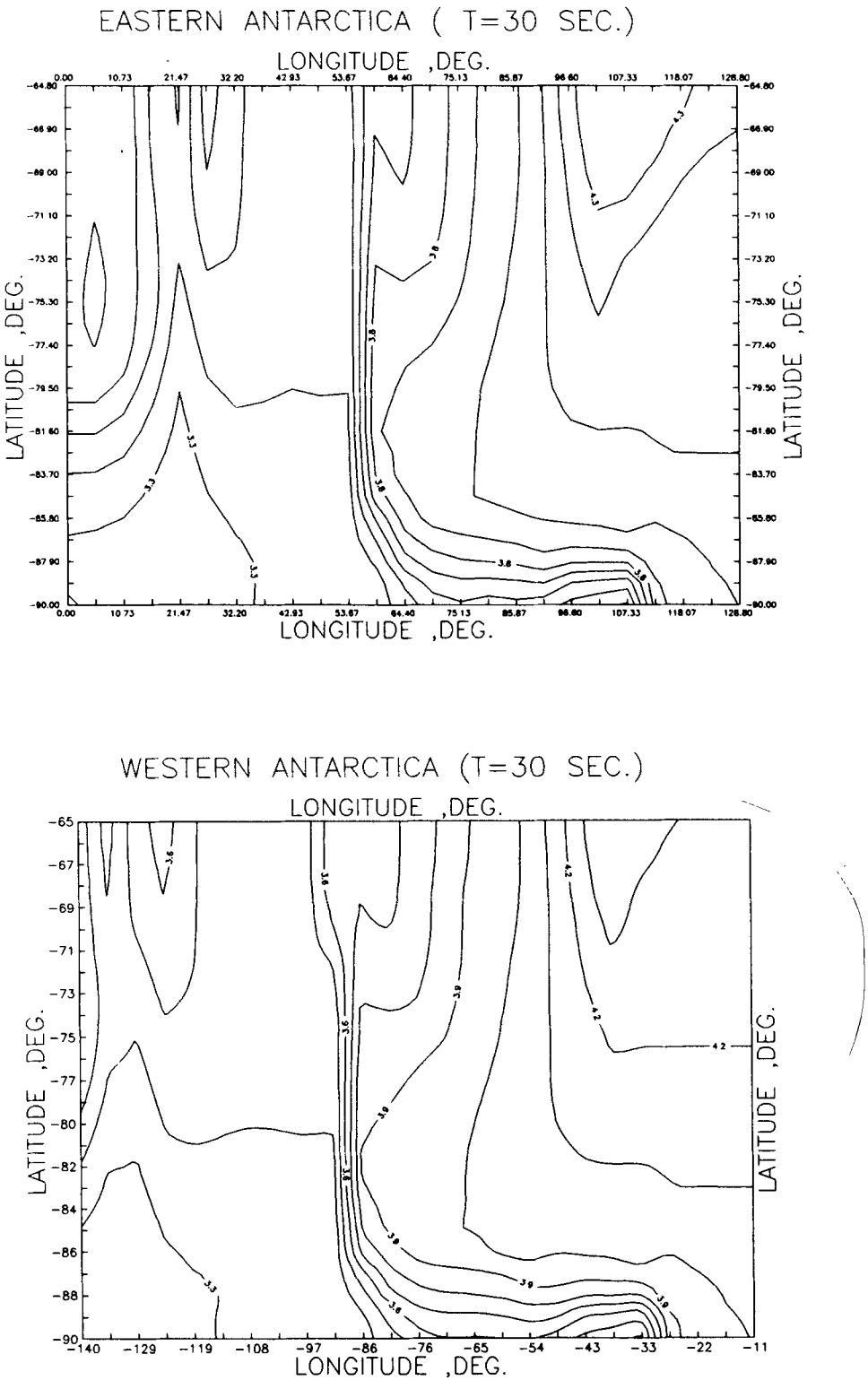

Figure 6. The pattern of lateral Rayleigh wave group velocity distribution resulting from the inversion at period of 30 s and 50 s for eastern and western Antarctica (after Yanovskaya *et al.* 1988).

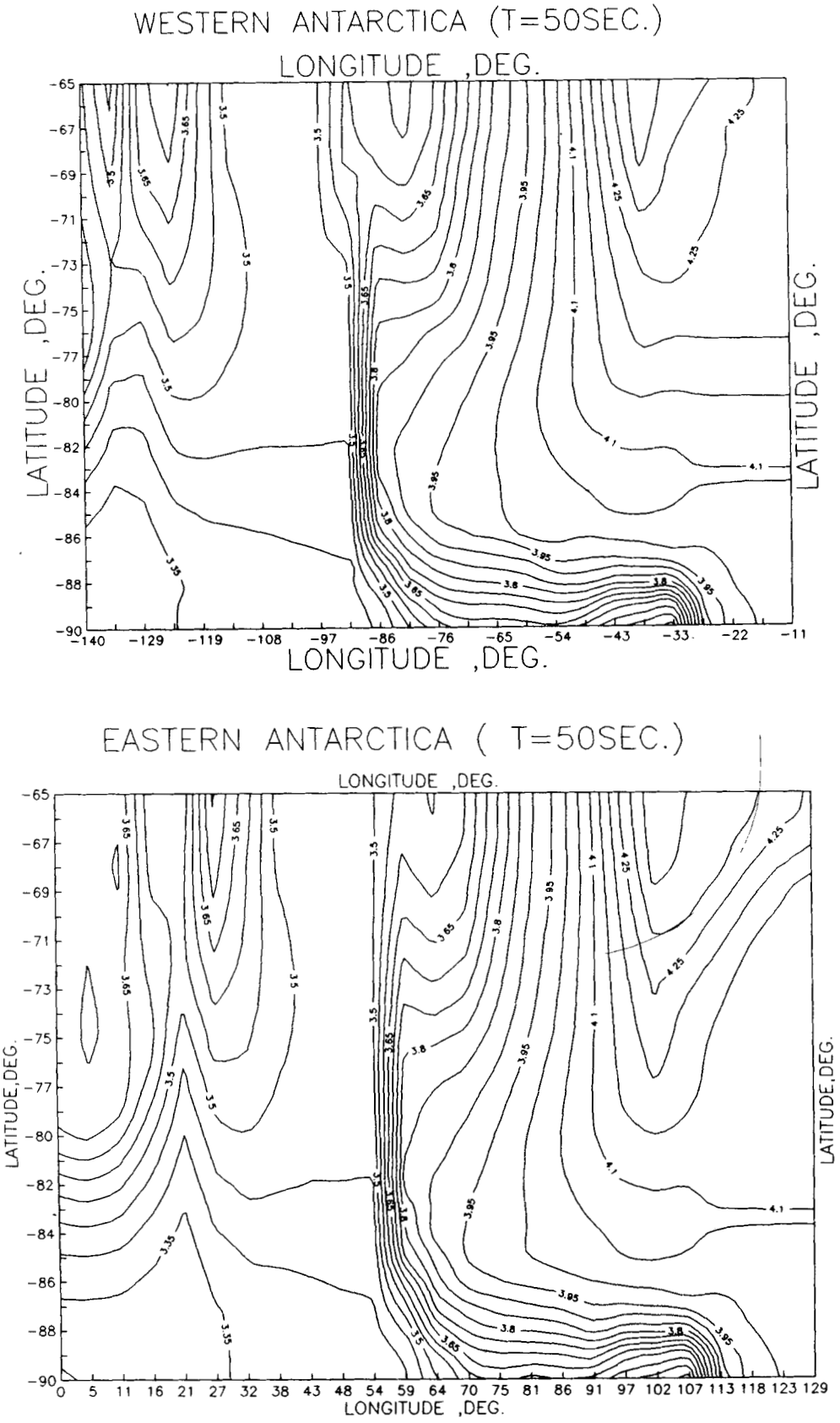

Figure 6. (*Continued.*)

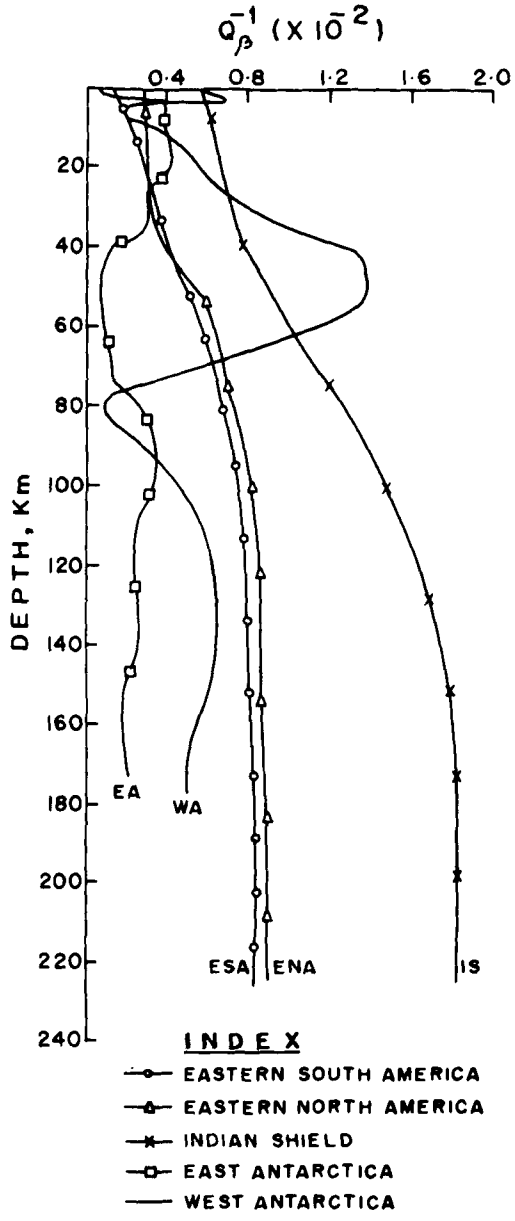

Figure 7. Comparison of Q_β^{-1} models for eastern (EA) and western (WA) Antarctica (obtained in this study) with the eastern south American (ESA), eastern north American (ENA) and Indian shield (IS) models.

Figure 7 shows the comparison of Q_β^{-1} models for eastern and western Antarctica with the eastern south American (ESA), eastern north American (ENA) and Indian shield (IS) models of Hwang & Mitchell (1987). In general Q_β^{-1} models show that there is a significant increase in Q_β^{-1} values in the asthenosphere compared to the lithosphere. There is a decrease in Q_β^{-1} values in the asthenosphere compared to lithosphere for Antarctica (Fig. 5). This shows the cooler asthenosphere compared to other stable shield regions of the world. A high attenuation zone ($Q = 65$) occurs at a depth of 20 to 90 km beneath western Antarctica (Fig. 5). Hwang & Mitchell (1987) have determined the Q_β^{-1} models for the crust and upper mantle beneath the stable and tectonically active regions of the world. They have estimated the upper mantle Q values to be between 40 and 130 and the highest values occurring beneath the stable regions of eastern north and south America, and lowest values occurring beneath the tectonically active regions of the world.

ACKNOWLEDGMENTS

The author is thankful to Dr H. M. Iyer, of the US Geological Survey, Menlo Park, California, USA; Drs N. A. Sergeyeva and O. E. Starovoit of W.D.C., Solid Earth Physics, Academy of Sciences of Russia, for providing the microfilm of earthquakes used in the study; and Professor Brian J. Mitchell of Saint Louis University, USA for his Q-inversion program. I am grateful to Dr T. B. Yanovskaya, Institute of Physics, Leningrad State University, Leningrad, Russia for her computer program of the surface-wave tomography studies. The author is grateful to the anonymous reviewers for providing valuable suggestions for the improvement of the paper. I am thankful to Professor D. Guptasarma, Director, National Geophysical Research Institute, Hyderabad, India, for giving permission to publish the work.

REFERENCES

Anderson, D.L. & Archambeau, C.B., 1964. The anelasticity of the Earth, *J. geophys. Res.*, **69**, 2071–2084.

Anderson, D.L., Ben-Menahem, A. & Archambeau, C.B., 1965. Attenuation of seismic energy in the upper mantle, *J. geophys. Res.*, **70**, 1441–1448.

Backus, G. & Gilbert, F., 1970. Uniqueness in the inversion of inaccurate gross earth data, *Phil. Trans. R. Soc.*, A., **266**, 123–192.

Behrendt, J.C., Le Masurier, W.E., Cooper, A.K., Tessensehn, F., Trehu, A. & Damaske, D., 1991. Geophysical studies of the west Antarctic rift system, *Tectonics*, **10**, 1257–1273.

Berg, J.H., Moscati, R. J. & Herg, D. L., 1989. A petrologic geotherm from a continental rift in Antarctica, *Earth planet. Sci. Lett.*, **93**, 98–108.

Bloch, S., Hales, A.L. & Landisman, M., 1969. Velocities in the crust and upper mantle of southern Africa from multi-mode surface wave dispersion, *Bull. seism. Soc. Am.*, **59**, 1599–1629.

Brune, J.N. & Dorman, J., 1963. Seismic waves and earth structure in the Canadian shield, *Bull. seism. Soc. Am.*, **53**, 167–210.

Dewart, G. & Toksoz, M.N., 1965. Crustal structure in East Antarctica from surface wave dispersion, *Geophys. J. R. astr. Soc.*, **10**, 127–139.

Evison, F.F., Ingham, C.E., Orr, R.H. & Fe Fort, J.H., 1960. Thickness of the Earth's crust in Antarctica and the surrounding oceans, *Geophys. J. R. astr. Soc.*, **3**, 289–306.

Fitzgerald, P.G., Sanasdrford, M., Barrett, P.J. & Gleasbum, A.J.W., 1986. Asymmetric extensions associated with uplift and subsidence of the Transantarctic Mountains and Ross Embayment, *Earth planet. Sci. Lett.*, **18**, 67–78.

Gonez, J.H., Hales, A.L. & Muirhead, K.J., 1975. Analysis of extended periods of Rayleigh and Love wave dispersion across Australia, *Geophys. J. R. astr. Soc.*, **41**, 81–105.

Hagiwara, T., 1958. A note on the theory of electromagnetic seismograph, *Bull. Earthquake Res. Inst. Tokyo Univ.*, **36**, 139–164.

Harkrider, D.G., 1968. The perturbation of Love wave spectra, *Bull. seism. Soc. Am.*, **58**, 861–880.

Hwang, H.J. & Mitchell, B.J., 1987. Shear velocities, Q and the

frequency dependence of Q in stable and tectonically active regions from surface wave observations, *Geophys. J.R. astr. Soc.*, **90,** 575–613.

Knopoff, L. & Vane, G., 1978/79. Age of east Antarctica from surface wave dispesion, *Pure appl. Geophys.*, **117,** 806–815.

Kovach, R.L. & Press, F., 1961. Surface wave dispersion and crustal structure in Antarctica and the surrounding oceans, *Ann. Geofis.*, **14,** 211–224.

Lawson, C.L. & Hanson, R.J., 1974. *Solving least square problems,* Prentice-Hall, Englewood Cliffs, NJ.

Mitchell, B.J., 1975. Regional Rayleigh wave attenuation in North America, *J. geophys. Res.*, **80,** 4904–4915.

Mitchell, B.J., 1976. Anelasticity of the crust and upper mantle beneath the Pacific Ocean from the inversion of observed surface wave attenuation, *Geophys. J. R. astr. Soc.*, **46,** 521–534.

Nyman, D.C. & Landisman, M., 1977. The display equalizer filter for frequency time analysis, *Bull. seism. Soc. Am.*, **67,** 393–404.

Rodi, W.L., Glover, P. Li, R.M.C. & Alexander, S.S., 1975. A fast accurate method for computing group velocity partial derivatives from Rayleigh and Love waves, *Bull. seism. Soc. Am.*, **65,** 1105–1114.

Singh, D.D., 1987. Crust and upper mantle velocity structure beneath north and central India from the phase and group velocity of Rayleigh and Love waves, *Tectonophysics,* **139,** 187–203.

Singh, D.D., 1988. Quasicontinental oceanic structure beneath the Arabian Fan sediments from the observed surface wave dispersion studies, *Bull. seism. Soc. Am.*, **65,** 1510–1521.

Smith, A.G. & Drewry, D.J., 1984. Delayed phase change due to hot asthenosphere causes Transantarctic uplift, *Nature,* **309,** 536–538.

Stern, T.A. & ten Brink, U.S., 1989. Flexural uplift of the Transantarctic Mountains, *J. geophys. Res.*, **94,** 10 315–10 330.

Thomas, L., 1969. Rayleigh wave dispersion in Australia, *Bull. seism. Soc. Am.*, **59,** 167–182.

Yanovskaya, T.B., Maaz, R., Ditmar, P.G. & Neunhofer, H., 1988. A method for joint interpretation of the phase and group surface-wave velocities to estimate lateral variations of the Earth's structure, *Phys. Earth planet. Inter.*, **51,** 59–67.